J Mater Sci: Mater Electron (2017) 28:7854–7861
DOI 10.1007/s10854-017-6482-9

# Effects of the Zr concentration on transparent $Y_2O_3$ ceramics fabricated by vacuum pre-sintering and a subsequent HIP treatment

**Lin-Lin Zhu[1] · Young-Jo Park[1] · Lin Gan[1,2] · Shin-Il Go[1] · Ha-Neul Kim[1] · Jin-Myung Kim[1] · Jae-Woong Ko[1]**

Received: 23 November 2016 / Accepted: 25 January 2017 / Published online: 7 February 2017


**Abstract** Highly transparent $Y_2O_3$ ceramics doped with different Zr concentrations were successfully fabricated by vacuum pre-sintering at temperatures ranging from 1600 to 1800 °C combined with a subsequent hot-isostatic pressing (HIP) treatment using commercial powders as the starting materials. All of the 1 mol% Zr-doped $Y_2O_3$ ceramics exhibit very good optical quality. The sample with the highest transparency level was realized by vacuum sintering at 1650 °C for 4 h followed by a post-HIP treatment at 1450 °C lasting 5 h. It has a fine microstructure and the grain size is 1.48 μm. Furthermore, the in-line transmittance reaches 83.3% at 1100 nm (1.2 mm thickness). It was found that a relatively low vacuum sintering temperature (1650 °C) and relatively low Zr doping concentration (1 mol%) are more appropriate to achieve optimally transparent $Y_2O_3$ ceramics with a subsequent HIP treatment.

## 1 Introduction

Cubic $Y_2O_3$ is a promising material by virtue of its excellent physical and chemical properties, such as its high thermal stability, visible and infrared light transparency (0.2–8 μm), and high melting point of around 2430 °C [1, 2]. However, the $Y_2O_3$ single crystal undergoes a structural phase transformation from cubic to high-temperature hexagonal phase at approximately 2280 °C, making it extremely difficult to fabricate with sufficient optical quality to large size by traditional melt-growth technology. Transparent ceramic counterparts have attracted the interest of researchers and been explored in relation to infrared windows and other applications such as active laser host materials for lanthanide ions, refractory devices and for certain components of semiconductor devices, especially since the first laser demonstration of the Nd:YAG ceramic in 1995 [3].

The high melting point, however, contributes to the low sinterability of yttria. Many efforts have been made to achieve transparent $Y_2O_3$ ceramics with full densification. A significant number of sintering methods have been developed including pressureless sintering methods, such as atmosphere sintering [4], vacuum sintering [5]. Pressure sintering approaches such as hot pressing and hot-isostatic pressing (HIP) can also be used. HIP is an advanced sintering technique by which the materials are heated with the simultaneous application of isostatic inert gas pressure, providing more driving force to eliminate internal voids and microporosity. In recent decades, many studies have been carried out in relation to the fabrication of transparent ceramics via pressureless pre-sintering and a post HIP treatment [6, 7]. Ikesue et al. reported in 1996 that the IR-transparent Nd doped $HfO_2$–$Y_2O_3$ ceramics were sintered under vacuum and HIPed with a pore-free structure [6]. Zhang et al. fabricated highly transparent $Y_2O_3$ ceramics without additives by air pre-sintering at various temperatures combined with a post HIP treatment [7]. Another possible technique for enhancing the sintering of $Y_2O_3$ is doping with sintering additives such as $ZrO_2$, $Al_2O_3$, $La_2O_3$, $HfO_2$, and $ThO_2$. Among them, the addition of $ZrO_2$ can

✉ Young-Jo Park
yjpark87@kims.re.kr

[1] Engineering Ceramics Department, Korea Institute of Materials Science, 797 Changwondaero, Changwon, Gyeongnam 641-831, Republic of Korea

[2] Minstry of Education Key Laboratory for Green Preparation and Application of Fuctional Materials, School of Material Science and Engineering, Hubei Collaborative Innovation Center for Advanced Organic Chemical Materials, Hubei University, 368 Youyi Avenue, Wuhan 430062, Hubei, China

improve the transmittance remarkably and inhibit the grain growth of the $Y_2O_3$ ceramics effectively, resulting in a homogeneous microstructure [8]. A smaller grain size benefits the mechanical properties and facilitates a pore release given the increased number of grain boundaries [9, 10]. However, this process requires a relatively high sintering temperature and a long holding time. Hou et al. successfully obtained highly transparent ceramics with different Zr doping concentrations at 1860 °C for 8 h in a vacuum atmosphere [5].

Many wet chemical routes are frequently utilized in the synthesis of starting powders for ceramic preparation but not suitable for scalable production [11–13]. The authors' preliminary study found that the pre-sintering process has a significant effect on the transparency of HIPed samples with 5 mol% Zr using commercially available $Y_2O_3$ and $ZrO_2$ powders as starting materials. However, the transmittance of the samples is not ideal and the effect of Zr doping concentration on the sinterability was not discussed [14].

In this work, highly transparent $Y_2O_3$ ceramics were fabricated using a combination of vacuum pre-sintering and a subsequent HIP treatment with using inexpensive commercial $Y_2O_3$ raw powders and $ZrO(CH_3COO)_2$ as a sintering additive. The effects of the sintering additive concentration and the vacuum pre-sintering temperature on the density, microstructure and optical properties were investigated in detail.

## 2 Experimental procedure

Commercial oxide powders of $Y_2O_3$ (99.99%, grain size ~1.2 μm, Rare Metallic Co Ltd., Tokyo, Japan) and $ZrO(CH_3COO)_2$ (98%, High Purity Chemicals, Sakado, Japan) were used as raw materials. Based on the formula of $(Y_{1-x}Zr_x)_2O_3$ ($x=0$, 0.01, 0.03, 0.05), the powders were weighed and milled with $ZrO_2$ balls in anhydrous alcohol (99.9%, Samchun, Pyeongtaek, Korea) for 24 h. After the milled slurry was dried by a rotary evaporator at 80 °C, the powder mixture was ground and sieved through a 150-mesh screen and then calcined at 800 °C for 4 h to remove organic components. The calcined powders were uniaxially pressed 5 MPa into Φ18 mm disks in a steel mold and further cold-isostatically pressed (CIP) at 200 MPa. The as-obtained green bodies were sintered at 1600–1800 °C for 4 h in a tungsten furnace under a vacuum of $1.0\times10^{-3}$ Pa. After sintering, the samples were HIPed at 1450 °C for 5 h under an Ar gas pressure of 180 MPa to obtain transparency.

The overall structure of the samples was determined through X-ray diffraction (XRD; D/Max 2500, Rigaku, Tokyo, Japan) analysis using $CuK_\alpha$ radiation ($\lambda=1.5406$ Å) at 40 kV and 100 mA. A step size of 0.01° was used with a scan speed of 6°/min. The in-line transmittance was measured by an UV–VIS–NIR spectrophotometer (Cary 5000, Varian, USA) over the wavelength region of 200–2500 nm. The density of the samples was measured by the Archimedes method using $H_2O$ as the immersion medium. The microstructures of fracture surface of the specimens were observed by a scanning electron microscope (SEM, JSM-6700F, JEOL, Tokyo, Japan). Field emission scanning electron microscopy (JSM-7001, JEOL, Tokyo, Japan) and energy dispersive spectroscopy (EDS) were used to analyze the polished surface and components of samples. The average grain size was examined by the intercept method using the equation $G=1.56$ L where $G$ is the average grain size and $L$ is the average intercept length.

## 3 Results and discussion

Figure 1a displays the XRD patterns of the $Y_2O_3$ ceramics doped with different Zr concentrations sintered at 1600 °C for 4 h in a vacuum. Z0, Z1, Z3 and Z5 represent the 0, 1, 3 and 5 mol% Zr concentration in the samples, respectively (see Table 1). All of the peaks of the doped and undoped samples perfectly match the standard cubic $Y_2O_3$ phase (JCPDS card, No. 41-1105) with a space group of Ia-3 without the presence of the $ZrO_2$ phase or other impurities. Upon a careful examination, the peaks were found to shift to higher angles gradually with an increase in the Zr concentration (Fig. 1b shows the peak shift between 28–30°), in accordance with the lattice parameter variations of the sintered $Y_2O_3$ ceramics as summarized in Table 1. The lattice parameters decrease slightly due to the smaller radius of $Zr^{4+}$ ($R=0.79$ Å) than that of $Y^{3+}$ ($R=0.89$ Å). The theoretical densities of the samples can be calculated according to the lattice parameters, which increase with the Zr concentration (Table 1).

The relative densities of sintered bodies with different Zr concentrations before and after the HIP treatment are shown as a function of the initial vacuum pre-sintering temperature in Fig. 2. When the doping concentration of Zr increases from 1 to 5 mol%, the relative densities of the specimens vacuum sintered at 1600 °C decrease from 93.3 to 73.9% in Fig. 2a. When the vacuum pre-sintering temperature exceeds 1700 °C, the Z0–Z5 specimens all show similar relative densities. The appearances of samples after vacuum pre-sintering are described in Table 2. The Z0 samples pre-sintered at different temperatures are all opaque and exhibit a minimal relative density differential of approximately 99.5%, while the Z1–Z5 samples become translucent with an increment in the sintering temperature. After the post-HIP treatment, the relative densities of the Z1–Z5 samples vacuum-pre-sintered at relatively low

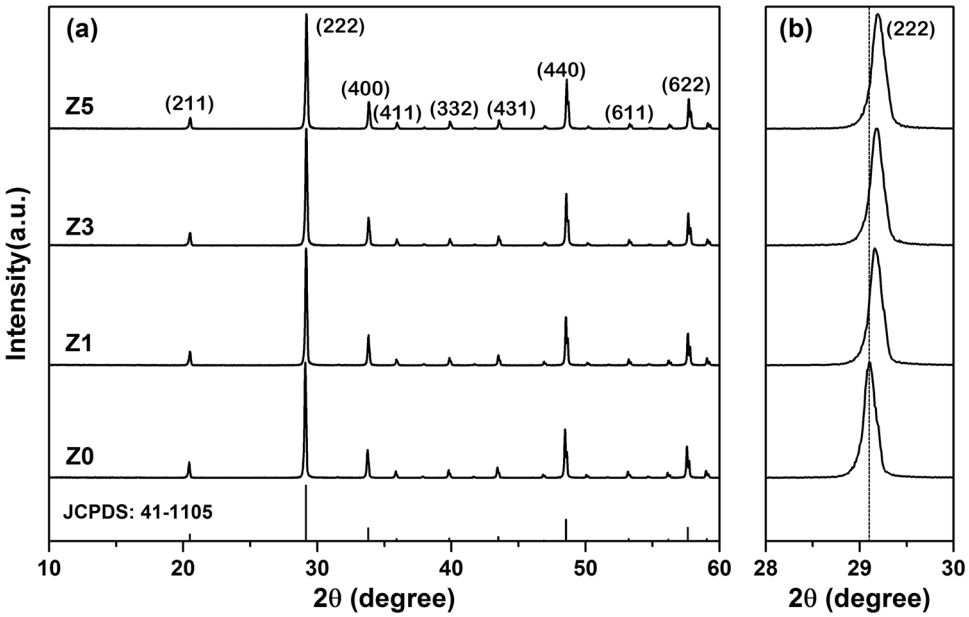


**Fig. 1** **a** X-ray diffraction patterns of $Y_2O_3$ ceramics doped with different Zr concentrations sintered at 1600 °C for 4 h in a vacuum atmosphere. **b** Magnification of the XRD patterns in the 2θ range of 28–30°

**Table 1** The lattice parameter (a = b = c) and density of cubic $Y_2O_3$ doped with different Zr concentrations

| Sample name | Zr concentration (mol%) | Lattice parameter (Å) | Calculated density (g/cm$^3$) |
|---|---|---|---|
| Z0 | 0 | 10.6118 | 5.020 |
| Z1 | 1 | 10.6091 | 5.029 |
| Z3 | 3 | 10.6025 | 5.047 |
| Z5 | 5 | 10.5973 | 5.064 |

temperatures are greatly improved. In addition, the samples pre-sintered at higher temperatures show a slight improvement in the relative density.

SEM micrographs of the microstructures of the Z0–Z5 samples vacuum-pre-sintered at 1650 °C for 4 h are shown in Fig. 3. Compared to the samples with Zr doping, Z0 clearly has larger grains and smaller intergranular pores, as presented in Fig. 3a. Meanwhile, several intragranular pores were also found, these can be attributed to the rapid grain growth. The Z1–Z5 samples (Fig. 3b–d) with Zr doping possess many large remnant intergranular pores with a similar grain size around 1 μm. Moreover, with an increase in the Zr concentration, the number of pores increases, which is consistent with the decreasing relative density results shown in Fig. 2a.

When the vacuum pre-sintering temperature increases to 1800 °C, relatively large intragranular pores exist in the

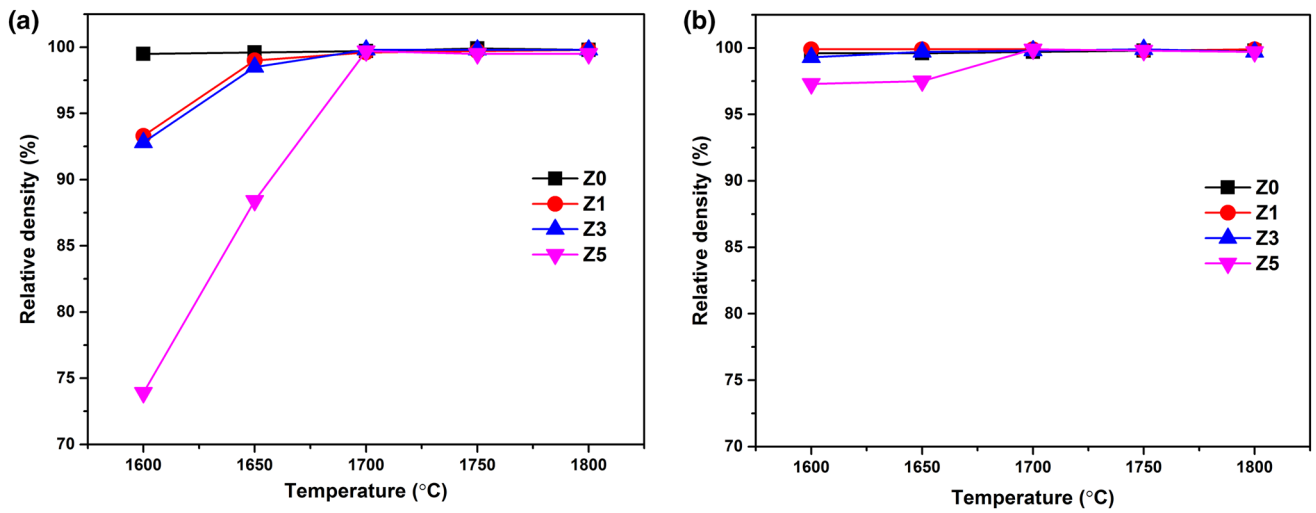


**Fig. 2** Relative densities of $Y_2O_3$ with different Zr doping concentrations after **a** vacuum pre-sintering and **b** a post-HIP treatment at 1450 °C

**Table 2** The appearances of Zr-doped samples after vacuum pre-sintering at various temperatures for 4 h

| Sample name | 1600 °C | 1650 °C | 1700 °C | 1750 °C | 1800 °C |
|---|---|---|---|---|---|
| Z0 | Opaque | Opaque | Opaque | Opaque | Opaque |
| Z1 | Opaque | Translucent | Translucent | Translucent | Translucent |
| Z3 | Opaque | Opaque | Translucent | Translucent | Translucent |
| Z5 | Opaque | Opaque | Translucent | Translucent | Translucent |

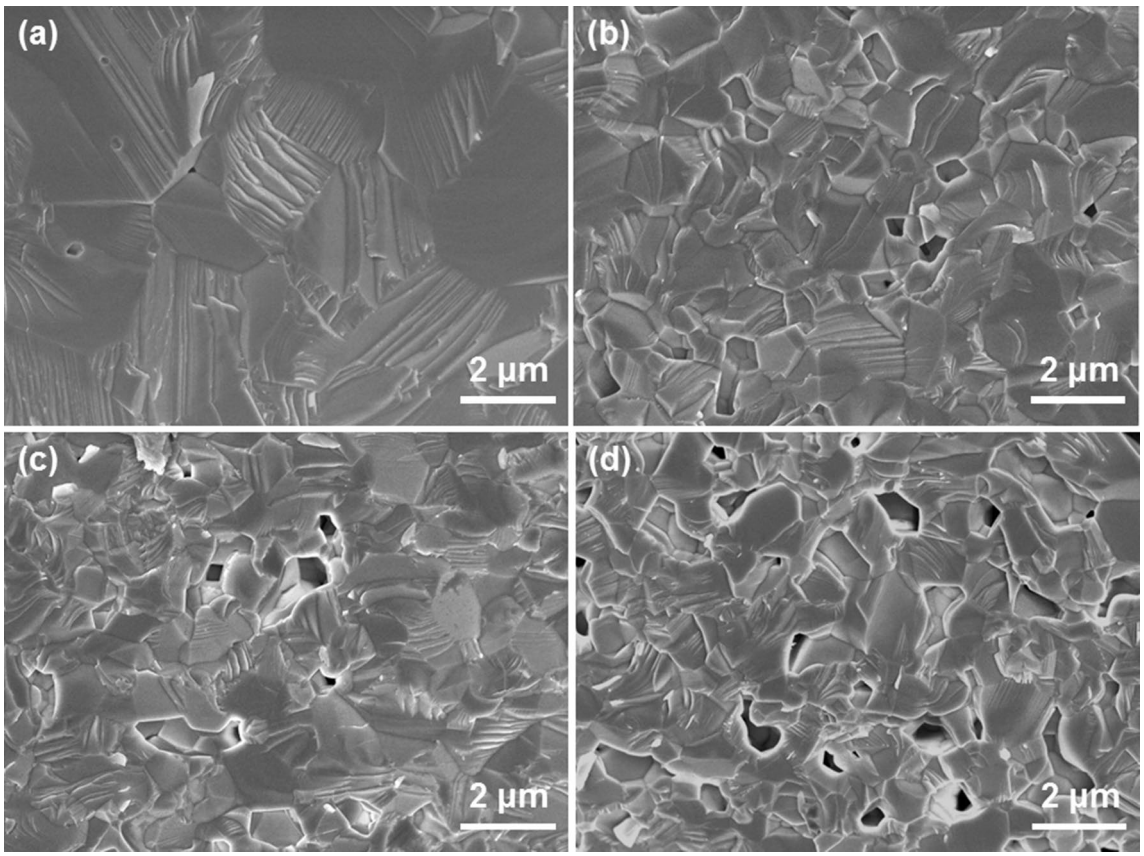


**Fig. 3** SEM micrographs of the fracture surfaces of vacuum-pre-sintered $Y_2O_3$ ceramics at 1650 °C for 4 h with different Zr contents **a** Z0, **b** Z1, **c** Z3, and **d** Z5

Z0 ceramic, as shown in Fig. 4a, whereas only a few small intergranular pores can be found in the Z1–Z5 ceramics as indicated by the white arrow. Moreover, the grain size decreases with an increase in the Zr doping concentration. Consequently, Zr doping can improve the densification behavior. This is most likely attributable to the uniformly fine microstructure and the smaller number of pores.

After the subsequent HIP treatment (Fig. 5), the microstructure differs somewhat from that of the samples pre-sintered at 1650 °C (Fig. 3) with different Zr doping concentrations. The Z1 sample (Fig. 5b), is fully densified with a nearly perfect pore-free microstructure, while for the samples with higher doping concentration Z3, there are some pores inside and, in particular, a large number of intergranular pores are still visible in the Z5 sample which may be due to the low density of the pre-sintered body [15]. Nevertheless, without an additive, some small intragranular pores remain after HIPing in both of the Z0 samples pre-sintered at 1650 and 1800 °C (Fig. 6a). No pores were observed after HIPing in the Z1–Z5 ceramics pre-sintered at 1800 °C (Fig. 6b–d), indicating that the relative density was improved slightly after the subsequent HIP treatment, as shown in Fig. 2. The main driving force during the HIP process for further densification is the mechanical stress provided by pressurizing argon [16], which will help to remove residual intergranular pores from Zr-doped samples but will not help Z0 samples with intragranular pores. Therefore, it is deduced that during the subsequent HIP treatment, a reduction of the porosity content reduction and shrinkage of the intergranular pores occurs predominantly

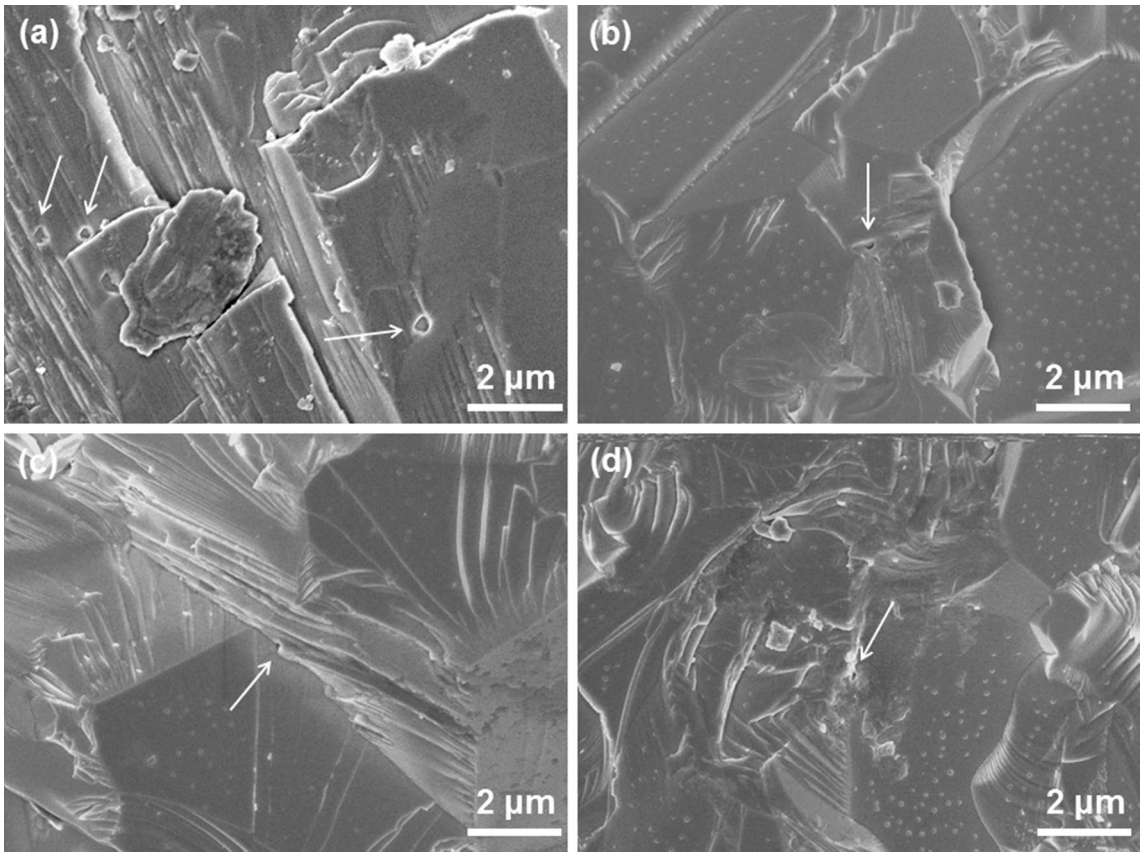


**Fig. 4** SEM micrographs of the fracture surfaces of vacuum-pre-sintered $Y_2O_3$ ceramics at 1800 °C for 4 h with different Zr concentrations **a** Z0, **b** Z1, **c** Z3, and **d** Z5

for Zr-doped $Y_2O_3$ ceramics pre-sintered at these two temperatures. With an increase in the Zr doping concentration, the grain sizes of the samples decrease. A previous study revealed that in $Y_2O_3$, grain boundary mobility is controlled by cation diffusivity, and cations diffuse by an interstitial mechanism [17]. For Zr-doped samples, two tetravalent $Zr^{4+}$ substitution cations tend to introduce one oxygen interstitial $O_i''$ the presence of which can inhibit the mobility of grain boundary. With an increase in the Zr doping concentration, the number of oxygen interstitials $O_i''$ in the samples increases. Because densification and grain growth are attributed to lattice and/or grain boundary diffusion [18], an increase in the Zr doping concentration leads to a decrease in the relative density, a smaller grain size and more residual pores.

Figure 7 shows the in-line transmittance spectrum of the Z1 ceramic vacuum-pre-sintered at 1650 °C for 4 h and then HIPed at 1450 °C for 5 h (1.2 mm in thickness). The inset shows the dependence of the in-line transmittance versus the vacuum pre-sintering temperature centered at 1100 and 400 nm. It is important to note that the Z1 samples vacuum pre-sintered at various temperatures have very good in-line transmittance which exceeds 80% at a wavelength of 1100 nm. The optimum values are 83.3% at 1100 nm and 76.9% at 400 nm when the Z1 specimen was vacuum-pre-sintered at 1650 °C for 4 h and then HIPed at 1450 °C for 5 h. Furthermore, the in-line transmittance of the Z1–Z5 ceramics with a subsequent HIP treatment in the near-infrared region increases with a decrease in the Zr concentration at an identical vacuum pre-sintering temperature below 1700 °C, corresponding to the behavior of the relative density and microstructure before and after the HIP treatment. When the samples with higher Zr doping concentration were vacuum-pre-sintered at 1800 °C, the corresponding in-line transmittance levels in the near-infrared region and especially in the visible region are not as good as those of samples pre-sintered at lower temperatures such as 1700 °C. Given that a relatively low pre-sintering-temperature always results in better light transmittance in the visible wavelength range [19], which is sensitive to the porosity and pore size, the small number of pores and defects which form in Zr-doped samples pre-sintered at a high temperature of 1800 °C may be difficult to remove by a further HIP treatment, as large grains decrease the area of grain boundary, thus decreasing the driving force to remove pores.

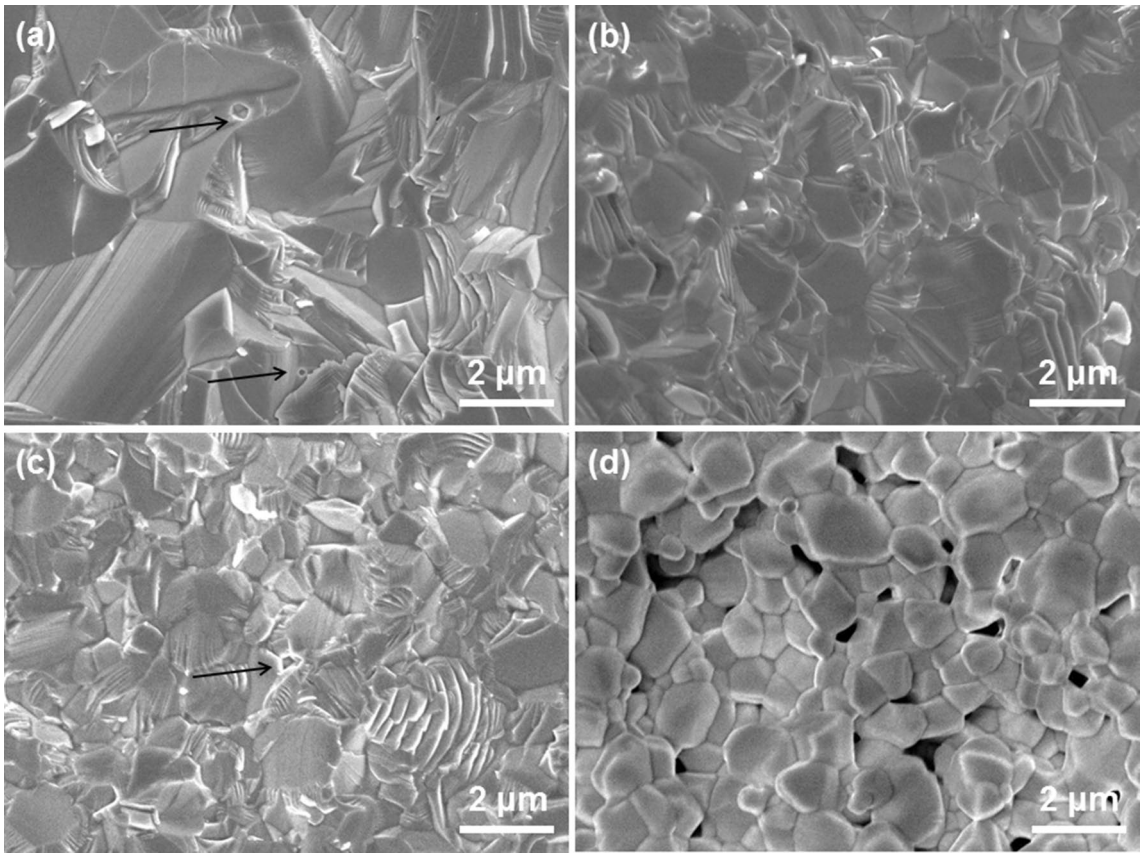


**Fig. 5** SEM micrographs of the fracture surfaces of HIPed $Y_2O_3$ ceramics pre-sintered at 1650 °C with different Zr contents **a** Z0, **b** Z1, **c** Z3, and **d** Z5

Figure 8a, d display the representative SEM micrographs of HIPed Z1 ceramics pre-sintered at 1650 °C (Fig. 8a) and 1800 °C (Fig. 8d) for 4 h. The average grain sizes of HIPed Z1 ceramics is 1.48 μm (1650 °C) and 4.18 μm (1800 °C). Because the average particle size of the $Y_2O_3$ raw powder is 1.2 μm, negligible grain growth occurs in HIPed Z1 transparent ceramic pre-sintered at 1650 °C. These two $Y_2O_3$ ceramics both exhibit high optical transmittance. With regard to the mechanical properties, a relatively low vacuum sintering temperature is recommended, which results in a much smaller grain size but equivalent transmittance (Fig. 7). Figure 8b, e exhibit the EDS spectra of HIPed Z1 ceramics pre-sintered at 1650 °C (Fig. 8b) and 1800 °C (Fig. 8e). There appeared no other emissions apart from Y, Zr, O, and C in the two samples. The elemental compositions of the samples in atom percent are given in Table 3. The Y and Zr atomic ratio in the samples is about 99:1, which is close to the nominal compositions. Figure 8c, f demonstrate the EDS mapping images of Zr element in the HIPed Z1 ceramics pre-sintered at 1650 °C (Fig. 8c) and 1800 °C (Fig. 8f). The Zr element is uniformly distributed in the samples.

## 4 Conclusions

In summary, $Y_2O_3$ ceramics with excellent optical transmittance were fabricated successfully by a combination of vacuum sintering and the HIP process using inexpensive commercial $Y_2O_3$ raw powders and $ZrO(CH_3COO)_2$ as sintering additive. With an increase in the Zr doping concentration, the relative density of the sintered body decreases. Moreover, the grain size decreases and is much smaller than that of a sample without a dopant at different sintering temperatures, providing evidence of the lack of rapid grain growth. In order to achieve highly transparent Zr-doped $Y_2O_3$ ceramics, a relatively low Zr doing concentration and a relatively low vacuum pre-sintering temperature but relatively high density are necessary for the subsequent HIP treatment. The optimum transmittance in the present work is 83.3% at 1100 nm and 76.9% at 400 nm when the Z1 specimen was vacuum-pre-sintered at 1650 °C for 4 h and then HIPed at 1450 °C for 5 h. The average grain size is 1.48 μm after the HIP treatment with an ultra-fine microstructure.

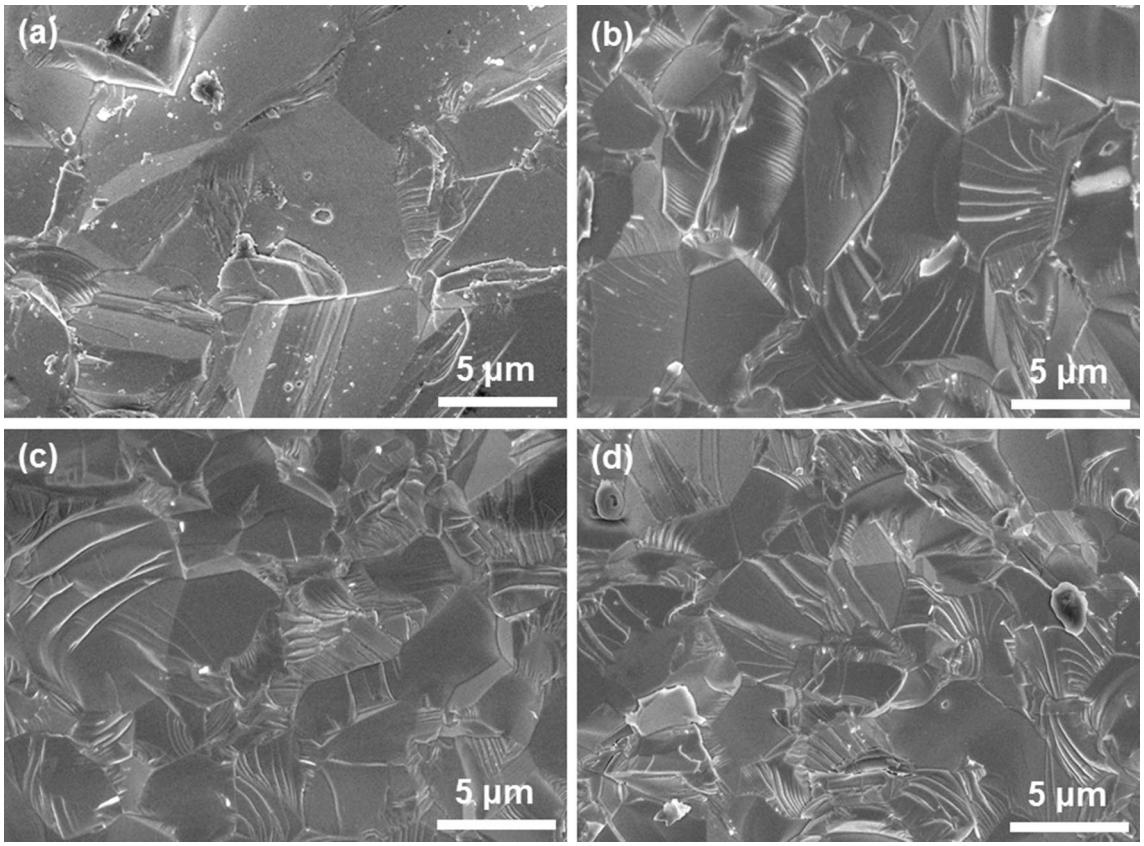


**Fig. 6** SEM micrographs of the fracture surfaces of HIPed $Y_2O_3$ ceramics pre-sintered at 1800 °C with different Zr contents **a** Z0, **b** Z1, **c** Z3, and **d** Z5

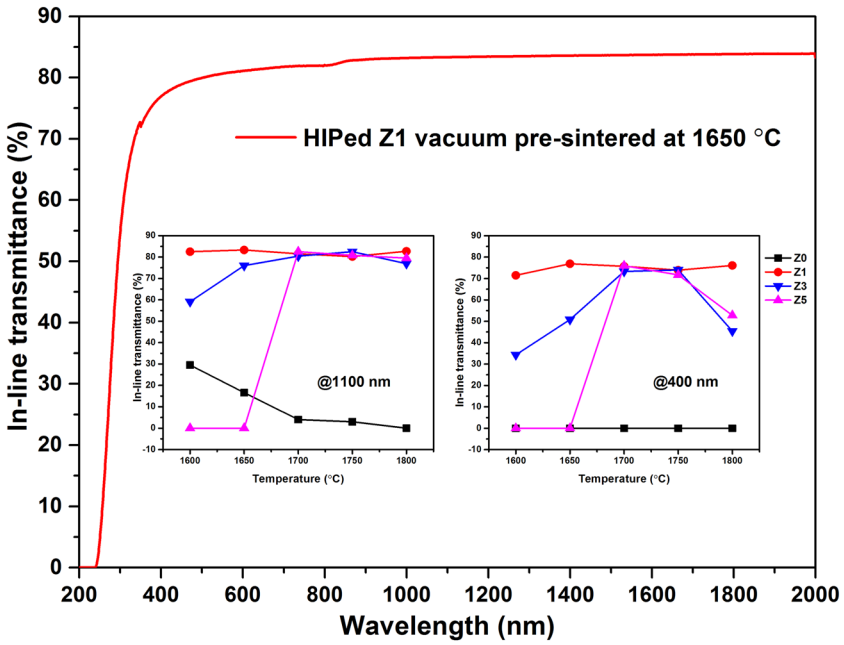


**Fig. 7** In-line transmittance spectrum of the Z1 ceramic vacuum-pre-sintered at 1650 °C for 4 h and then HIPed at 1450 °C for 5 h (1.2 mm in thickness). The *inset* shows dependence of the vacuum pre-sintering temperature versus the in-line transmittance centered at 400 (*left*) and 1100 nm (*right*)

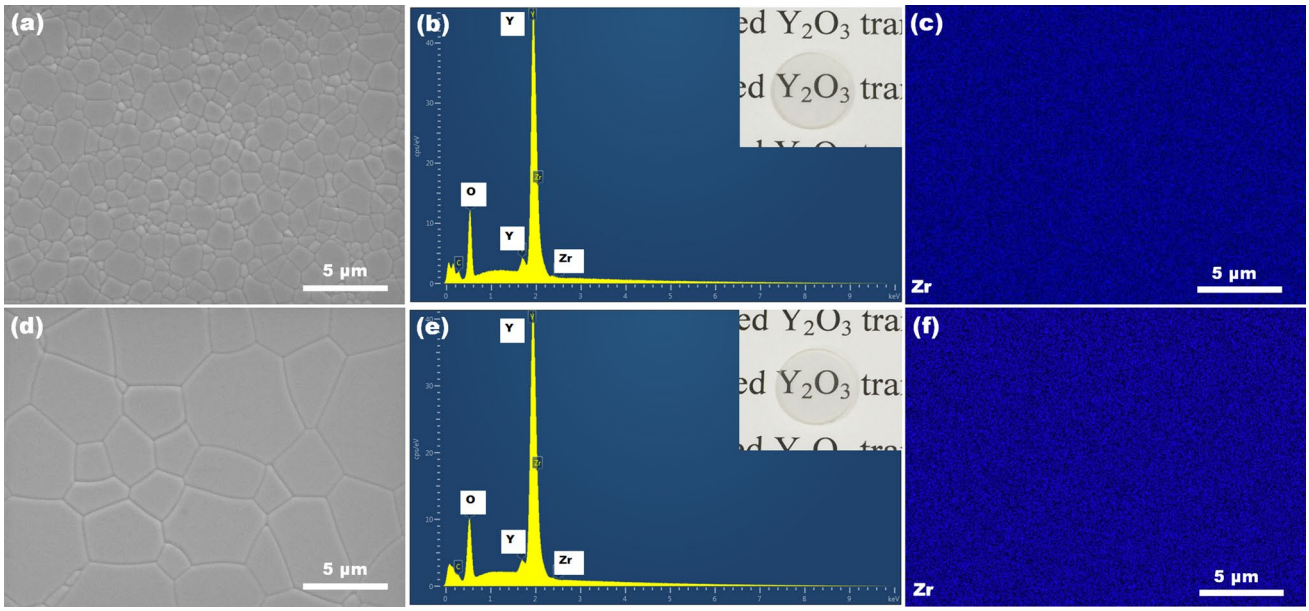


**Fig. 8** **a, d** SEM micrographs of the HIPed Z1 transparent ceramics pre-sintered at 1650 °C (**a**) and 1800 °C (**d**) for 4 h and the corresponding EDS spectra and EDS surface scanning of Zr element in the HIPed Z1 transparent ceramics pre-sintered at 1650 °C (**b–c**) and 1800 °C (**e–f**)

**Table 3** EDS estimation of elemental composition for HIPed Z1 transparent ceramics pre-sintered at 1650 °C and 1800 °C for 4 h

| Pre-sintering temperature | Y (atom%) | Zr (atom%) | Y:Zr (atomic ratio) |
|---|---|---|---|
| 1650 °C | 111.32 | 1.12 | 99.39 |
| 1800 °C | 111.32 | 1.13 | 98.60 |

**Acknowledgements** This work was supported by the Materials & Components Technology Development (MCTD) Program (PN: 10047010, Development of 80% Light-Transmitting Polycrystalline Ceramics for Transparent Armor·Window Applications) funded by the Ministry of Trade, Industry & Energy (MOTIE) of Korea.

## References

1. X.R. Hou, S.M. Zhou, T.T. Jia, H. Lin, H. Teng, J. Lumin. **131**, 1953–1958 (2011)
2. J.R. Lu, K. Takaichi, T. Uematsu, A. Shirakawa, M. Musha, K.i.. Ueda, H. Yagi, T. Yanagitani, A.A. Kaminskii, Jpn. J. Appl. Phys. **41**, L1373–L1375 (2002)
3. A. Ikesue, I. Furusato, J. Am. Ceram. Soc. **78**, 225–228 (1995)
4. G.G. Zhao, Q.H. Yang, Q. Liu, S.Z. Lu, J. Alloy. Compd. **583**, 372–375 (2014)
5. X.R. Hou, S.M. Zhou, Y.K. Li, W.J. Li, Opt. Mater. **32**, 920–923 (2010)
6. A. Ikesue, J. Am. Ceram. Soc. **2**, 359–364 (1996)
7. Z.Y. Wang, L. Zhang, H. Yang, J. Zhang, L.X. Wang, Q.T. Zhang, Ceram. Int. **42**, 4238–4245 (2016)
8. L.L. Jin, G.H. Zhou, S. Shimai, J. Zhang, S.W. Wang, J. Eur. Ceram. Soc. **30**, 2139–2143 (2010)
9. K. Serivalsatit, B. Kokuoz, B. Yazgan-Kokuoz, M. Kennedy, J. Ballato, J. Am. Ceram. Soc. **93**, 1320–1325 (2010)
10. G. Wang, V.D. Krstic, Philos. Mag. A **78**, 1125–1135 (1998)
11. M. Maddahfar, M. Ramezani, M. Sadeghi, A. Sobhani-Nasab, J. Mater. Sci.: Mater. Electron. **26**, 7745–7750 (2015)
12. M. Rahimi-Nasrabadi, M. Behpour, A. Sobhani-Nasab, S.M. Hosseinpour-Mashkani, J. Mater. Sci.: Mater. Electron. **26**, 9776–9781 (2015)
13. M. Sobhani-Nasab, M. Maddahfar, S.M. Hosseinpour-Mashkani, J. Mol. Liq. **216**, 1–5 (2016)
14. L. Gan, Y.J. Park, H.N. Kim, J.M. Kim, J.W. Ko, J.W. Lee, Ceram. Int. **41**, 9622–9627 (2015)
15. M. Descamps, L. Boilet, G. Moreau, A. Tricoteaux, J. Lu, A. Leriche, V. Lardot, F. Cambier, J. Eur. Ceram. Soc. **33**, 1263–1270 (2013)
16. M. Suárez, A. Fernández, J.L. Menéndez, M. Nygren, R. Torrecillas, Z. Zhao, J. Eur. Ceram. Soc. **30**, 1489–1494 (2010)
17. P.L. Chen, I.W. Chen, J. Am. Ceram. Soc. **79**, 1801–1809 (1996)
18. H. Yoshida, M. Kodo, K. Soga, T. Yamamoto, J. Eur. Ceram. Soc. **32**, 3103–3114 (2012)
19. S.N. Bagayev, A.A. Kaminskii, Y.L. Kopylov, V.B. Kravchenko, Opt. Mater. **33**, 702–705 (2011)